Fluorescence Spectroscopy of All-*trans*-anhydrorhodovibrin and Spirilloxanthin: Detection of the $1B_u^-$ Fluorescence

Ritsuko Fujii,[†] Tatsuya Ishikawa,[†] Yasushi Koyama,*[,†] Miwa Taguchi,[‡] Yoshie Isobe,[‡] Hiroyoshi Nagae,[§] and Yasutaka Watanabe[‡]

Departments of Chemistry and Physics, Faculty of Science, Kwansei Gakuin University, Uegahara, Nishinomiya 662-8501, Japan, and Kobe City University of Foreign Studies, Gakuen Higashi-Machi, Nishi-ku, Kobe 651-2187, Japan

Received: January 16, 2001; In Final Form: March 22, 2001

Fluorescence spectra of all-*trans*-anhydrorhodovibrin and spirilloxanthin having the number of conjugated double bonds $n = 12$ and 13 were recorded in *n*-hexane solution. The optically forbidden $2A_g^- \rightarrow 1A_g^-$ fluorescence was observed for carotenoids having such a long conjugated chain, and the optically forbidden $1B_u^- \rightarrow 1A_g^-$ fluorescence was identified for the first time. The proposed energies of the $2A_g^-$, $1B_u^-$, and $1B_u^+$ fluorescence origins are 12 500, 14 900, and 19 200 cm^{-1} for anhydrorhodovibrin and 11 900, 13 600, and 18 900 cm^{-1} for spirilloxanthin (at 295 K). The estimated transition dipole moments for fluorescence from the $2A_g^-$, $1B_u^-$, and $1B_u^+$ states to the ground $1A_g^-$ state are 1.24, 4.76, and 17.4 D for the former and 1.37, 3.72, and 16.8 D for the latter.

Introduction

In the light-harvesting function of carotenoid (Car), the following scheme of internal conversion within the Car and singlet-energy transfer from Car to bacteriochlorophyll (BChl) has been generally accepted:[1,2] Upon absorption of a photon, the Car is excited from the ground ($1A_g^-$) state to the optically allowed $1B_u^+$ state and internally converts to the $2A_g^-$ state and then to the ground $1A_g^-$ state. Competitively, the Car-to-BChl singlet-energy transfer reactions take place through two channels, i.e., one from the $1B_u^+$ state of Car to the Q_x state of BChl and the other from the $2A_g^-$ state of Car to the Q_y state of BChl. Here, the $1B_u^+$-to-$2A_g^-$ internal conversion plays a most important role in tuning the partition of energy flow through those two channels.

The approximate C_{2h} symmetry of the stretched conjugated chain of all-*trans*-Cars, which is ubiquitously present in the antenna complexes, gives rise to singlet states with different symmetries, i.e., $k\ A_g^+$, $l\ A_g^-$, $m\ B_u^+$ and $n\ B_u^-$. Here, optical transition is allowed between the A_g and B_u states having different Pariser's signs,[3,4] whereas vibronic coupling-mediated internal conversion is allowed between states having the same Pariser's signs.[5] Therefore, it turns out that the direct internal conversion from the $1B_u^+$ to the $2A_g^-$ state is symmetry-forbidden.[6,7]

Discovery of a new singlet state between the $1B_u^+$ and $2A_g^-$ states has provided us with a new insight into the scheme of internal conversion and singlet-energy transfer[5,8,9]: The PPP-MRD calculations of the singlet-state energies for shorter polyenes[10,11] predicted (i) the dependence of the state energies on the number of conjugated double bonds, *n*, as a function of $1/(2n + 1)$, (ii) the ordering of the low-lying singlet states, i.e., $1A_g^-$ (S_0) < $2A_g^-$ (S_1) < $1B_u^-$ (S_2) < $1B_u^+$ (S_3) for $n > 5$, and (iii) much stronger *n* dependence of the $1B_u^-$ energy than the $1B_u^+$ and $2A_g^-$ energies. The measurements of resonance-Raman excitation profiles of crystalline lycopene ($n = 11$), spheroidene ($n = 10$), and mini-9-β-carotene ($n = 9$) have proven that the above three predictions are actually the case, as shown in Figure 1a. The results lead us to a definitive assignment of this newly identified state to the $1B_u^-$ state.[5,8]

Now, we know that the $1B_u^-$ state can mediate the internal conversion from the $1B_u^+$ state eventually to the $2A_g^-$ state. Actually, sequential internal conversion processes of $1B_u^+ \rightarrow 1B_u^- \rightarrow 2A_g^-$ have been evidenced by subpicosecond time-resolved absorption spectroscopy of all-*trans*-neurosporene in both the visible[12] and near-infrared[13] regions. Possible mechanisms of this stepwise internal conversions have been proposed,[5] but they need to be established (see ref 9 for a review).

Here, an important question to be addressed is whether the $1B_u^-$ state is involved in the Car-to-BChl singlet-energy transfer: Because the Q_x-state energy of BChls is 16 900 cm^{-1} and the Q_y-state energy of the B800 (B850) BChl is 12 500 (11 800) cm^{-1} (see Figure 1a), the $1B_u^-$ state can potentially transfer its energy either to the Q_x or to the Q_y state. In addition to its lifetime, another important parameter is its oscillator strength, which determines the rate of singlet-energy transfer through the transition dipole−transition dipole mechanism.[14,15]

Extensive studies have been done to estimate the $2A_g^-$ energies by the use of the $2A_g^-$ lifetimes and the energy-gap law.[16−18] Most recently, the $2A_g^-$ energies of violaxanthin ($n = 9$) and zeaxanthin ($n = 11$) have been determined either by stationary-state fluorescence spectroscopy[19] or by subpicosecond absorption spectroscopy by the use of the $1B_u^+ \leftarrow 2A_g^-$ transition that appears in the near-infrared region.[20] Importantly, the $2A_g^-$-state energy of spheroidene bound to the LH2 complex has been determined by two-photon absorption spectroscopy.[21] However, attempts to spectroscopically determine the $2A_g^-$ energies by fluorescence spectroscopy[19,22−25] or by measure-

* To whom correspondence should be addressed. Prof. Yasushi Koyama Faculty of Science, Kwansei Gakuin University, 1-1-155 Uegahara, Nishinomiya 662-8501, Japan. Fax: +81-798-51-0914. Phone: +81-798-54-6389. E-mail: ykoyama@kwansei.ac.jp.

[†] Department of Chemistry, Kwansei Gakuin University.

[‡] Department of Physics, Kwansei Gakuin University.

[§] Kobe City University of Foreign Studies.

10.1021/jp010150b CCC: $20.00
Published on Web 05/12/2001

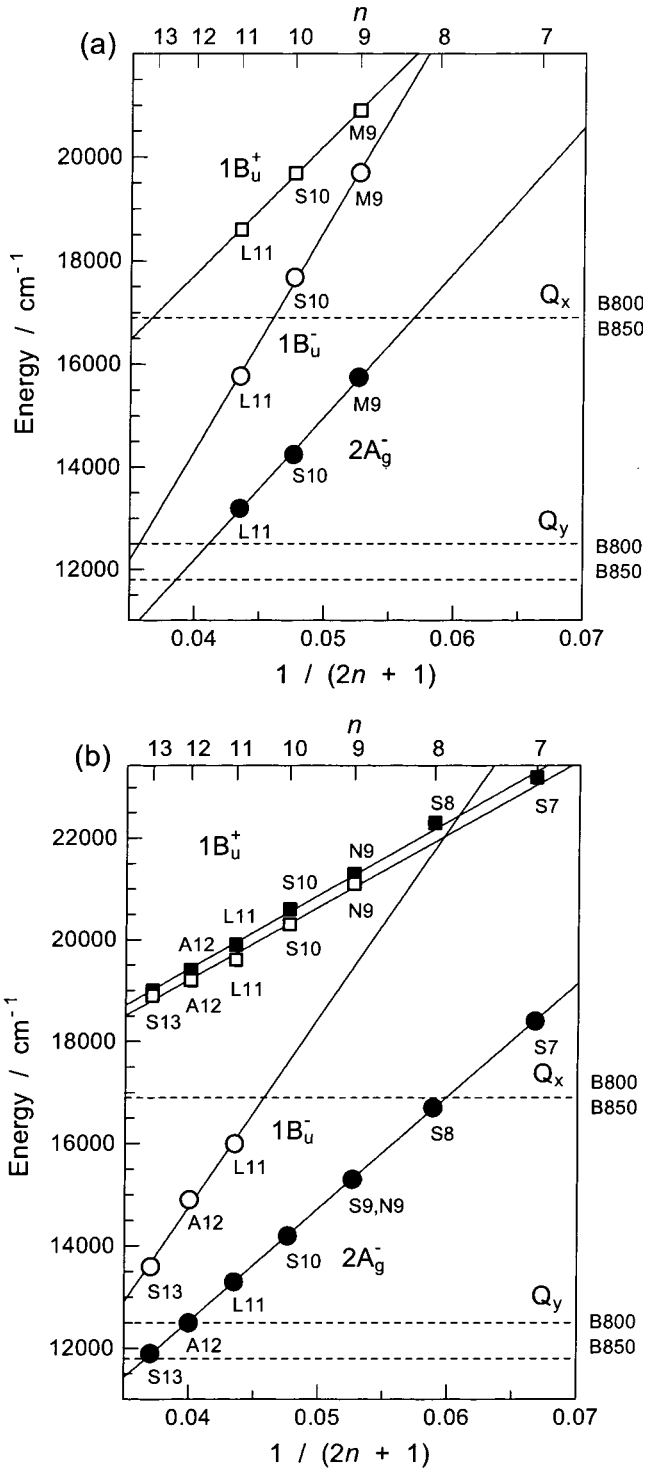

Figure 1. Dependence of the $1B_u^+$ (0), $1B_u^-$ (0), and $2A_g^-$ (0) energies of all-*trans*-Cars on the number of conjugated double bonds, *n*, as a function of $1/(2n + 1)$. (a) The state energies determined by measurements of resonance-Raman excitation-profiles in the crystalline state at 77 K[5,8,26] and (b) those determined by electronic-absorption and fluorescence spectroscopy in solution at 295 K.[23,25] In the latter, the $1B_u^+$ and $2A_g^-$ energies of spheroidene derivatives in methanol[22] are also included. Abbreviations of all-*trans*-Cars are as follows: S7, 3,4,7,8-tetrahydrospheroidene; S8, 3,4,5,6-tetrahydrospheroidene; S9, 3,4-dihydrospheroidene; N9, neurosporene; M9, mini-9-β-carotene; S10, spheroidene; L11, lycopene; A12, anhydrorhodovibrin; and S13, spirilloxanthin. Attached numerals indicate the number of conjugated double bonds. The energies of the Q_x and Q_y states in the LH2 antenna complexes are also shown for comparison.

ments of resonance-Raman excitation profiles[26] are still limited only for shorter-chain Cars ($n = 11$). On the other hand, the $1B_u^-$ state has been identified only by the measurements of resonance-Raman excitation profiles for Cars ($n = 9-11$).[5,8]

In the present investigation, we have attempted to detect the optically forbidden $2A_g^- \rightarrow 1A_g^-$ fluorescence in the near-infrared region from photosynthetic Cars having a longest conjugated chain, i.e., all-*trans*-anhydrorhodovibrin ($n = 12$) and spirilloxanthin ($n = 13$), after developing the method of sample purification and up-grading our setup for detecting weak fluorescence in the near-infrared region. We also tried to detect the optically forbidden $1B_u^- \rightarrow 1A_g^-$ fluorescence of such long-chain Cars, which is hopefully shifted to the low-energy side, and may not be completely covered with the strongly optically allowed $1B_u^+ \rightarrow 1A_g^-$ fluorescence. We tried to determine the important parameters mentioned above, including the energies, the shifts of the excited-state potentials, and the transition dipole moments of the $1B_u^-$ and $2A_g^-$ states, which are absolutely necessary to determine the mechanisms of internal conversion within the Car and those of the singlet-energy transfer reactions to BChl. Here, we took full advantage of our previous experience in analyzing the fluorescence spectra of shorter-chain Cars, i.e., all-*trans*-neurosporene, spheroidene,[23] β-carotene,[24] and lycopene[25] in challenging the analyses of the fluorescence spectra of the present Cars that are expected to be much more complicated.

Experimental Section

Sample Preparation. All-*trans*-spirilloxanthin and anhydrorhodovibrin were isolated from *Allochromatium vinosum* strain D that was anaerobically grown in "the inorganic medium for *Chromatium*"[27] at 30 °C for a week. Cold methanol (~400 mL) was added to the packed cells (~40 g) and then stirred at ~4 °C for 30 min in the dark under N_2 atmosphere. After centrifugation of the suspension to remove the BChl solution (10 000 ×g, 5 min), a mixture of cold acetone/methanol (7/2; ~400 mL), containing a small amount of ascorbic acid, was added to the residue and stirred to extract Cars. After centrifugation of the mixture (10 000 ×g, 5 min), the supernatant was collected and tetrahydrofuran (THF; ~200 mL) was added to the residue to extract Cars again. These extracts were mixed with each other, and the Car component was transferred to the petroleum ether (p-ether) layer (~300 mL) by funnel separation against aqueous solution of sodium chloride (~300 mL). After being dried over anhydrous sodium sulfate, the p-ether layer was concentrated and then *n*-hexane was added to the remaining solution to partially replace p-ether by *n*-hexane. This procedure was quickly repeated several times. Then, the solution was loaded onto an alumina column (Merck, Alumina Oxide 90, activity II~III) equilibrated with *n*-hexane. The remaining BChl *a* and its degradation products stayed on the top of the column, and a mixture of anhydrorhodovibrin and spirilloxanthin eluted with 10−20% diethyl ether in *n*-hexane. After repeating, several times, concentration of the solution and subsequent dilution with *n*-hexane, the mixture was subjected to alumina column chromatography again. Anhydrorhodovibrin (spirilloxanthin) was eluted with 10% (15−20%) diethyl ether in *n*-hexane. The collected anhydrorhodovibrin (spirilloxanthin) was then crystallized at −30 °C in 5% (30%) THF in *n*-hexane.

Just before the fluorescence measurement of anhydrorhodovibrin, fresh crystals of the all-*trans* isomer (~1.5 mg) were dissolved in *n*-hexane and purified by silica gel (Merck, Si-60) column chromatography using 1% 2-propanol in *n*-hexane as eluent and then by alumina column chromatography using 5−10% diethyl ether in *n*-hexane as eluent. All-*trans*-anhy-

drorhodovibrin immediately after this purification was dissolved in *n*-hexane (Dojin Chemicals, Kumamoto, for fluorescence spectroscopy) or 3-methyl pentane (Tokyo Kasei Kogyo Co. Ltd., Tokyo) at a concentration of 6×10^{-6} M.

In the fluorescence measurements of spirilloxanthin, a large amount of crystals (>10 mg) that had been grown in 30% THF/*n*-hexane solution were washed with *n*-hexane several times and then dissolved into a mixture of 5% benzene (Kishida Chemical Co. Ltd., Osaka, for spectroscopy) in 3-methyl pentane at a concentration of $6-8 \times 10^{-6}$ M.

Fluorescence Spectroscopy. A homemade setup for electronic-absorption, fluorescence measurements described previously[23-25,28] was up-graded as follows: Each sample solution sealed into a quartz tube (4 mm i.d.) was mounted in a closed-cycle helium cryostat (Leybold-Heraens, ROK 10−300 & RW2), and its temperature was controlled in the range of 10−300 K by the use of a thermostat (Scientific Instruments, Model 9650).

(a) Electronic-absorption measurements. As a light source, the output of a 300 W I_2 lamp (Ushio JC-24V) was used after passing through a double monochromator (JUSCO M25D, equipped with a 1200 line/mm and 500 nm blaze grating, the entrance/exit slits 1.0−2.0 mm) and then a filter (Toshiba UV 31). The incident beam was focused onto the sample, and the transmitting light was detected by a photomultiplier (Hamamatsu R632).

(b) Fluorescence measurements. As a fixed-wavelength light source for ordinary fluorescence measurements, the 488 nm beam from a combination of an Ar^+ laser (NEC GLG 3050, 5 or 10 mW) and a spectrometer (Spectrolab, Laser SpecIII) was used. Each incident beam was focused onto the sample tube with a different set of lenses.

The fluorescence was detected as follows: In the visible region, a 90° emission was collected after passing through a glass filter (Toshiba VY50) and focused onto the entrance slit (0.3−2.5 mm) of a single monochromator (JASCO CT25C, equipped with a 1200 line/mm and 500 nm blaze grating), and the output was detected by a GaAs photocathode detector (Hamamatsu R943−02), hereafter denoted as "PM1". The power of excitation was monitored, for a split beam, by the use of an S1-type photomultiplier (Hamamatsu R1463P), denoted as "PM2". Both photomultipliers were directly cooled with liquid nitrogen to minimize the dark counts. The output signals from PM1 and PM2 were sent to a pair of amplifier and discriminator (PARC 1121) and then to a photon counter (PARC 1109). Here, fluorescence was recorded in a mode compensating the fluctuation of the light source; the gate of PM1 was open during a period when a specified count was accumulated through PM2. The fluorescence and fluorescence-excitation data were corrected for an instrumental function that had been determined by the use of a standard lamp. No spectral smoothing was performed.

In the near-infrared region, the 488 nm beam was chopped with 25 ms open−close cycle. The open−close information detected by an oscilloscope was sent to a photon counter (SSR 1120). A 90° emission from the sample was collected after passing through a glass filter (Toshiba R68) and focused onto the entrance slit (3.0 mm) of a single monochromator (JASCO M10-TP with a 10 cm focal length, equipped with a 600 line/mm and 1000 nm blaze grating), and the output was detected by an InP/InGaAs photomultiplier (Hamamatsu R5509−71). The output signal was sent to an amplifier and discriminator (SSR 1105) and then to the photon counter (SSR 1120). Each signal when the chopper was in the close mode was subtracted from the signal when the chopper was in the open mode, and then the difference was accumulated for 5−10 s. Although the dark count of this photomultiplier was 700 cps at 140 K, the practical dark count became less than 10 cps after this procedure.

Results and Discussion

Decomposition of the Fluorescence Spectra into the $1B_u^+$, $1B_u^-$, and $2A_g^-$ Fluorescence Progressions. In previous analyses of the fluorescence spectra of all-*trans*-neurosporene ($n = 9$) and spheroidene ($n = 10$),[23] no clear indication of the $1B_u^-$ state was seen. In both cases, extension of the $1B_u^+$ and the $2A_g^-$ fluorescence progressions to the lower-energy side could explain the entire fluorescence profile. In the present analyses of the fluorescence spectra of all-*trans*-anhydrorhodovibrin ($n = 12$) and spirilloxanthin ($n = 13$), introduction of the $1B_u^-$ fluorescence progression became necessary to explain the entire profile. However, because of the severe overlap of all of the $1B_u^+$, $1B_u^-$, and $2A_g^-$ fluorescence progressions, we had to make the following assumptions that are based on our previous analyses of the shorter-chain Cars: (i) Each vibronic peak has a Gaussian shape. (ii) The spacings between a pair of vibronic peaks are almost the same for all of the three fluorescence progressions reflecting the ground-state vibrational levels. The spacing can be smaller for transitions to higher vibrational levels because of the unharmonicity of the ground-state potential. (iii) The bandwidth of the vibronic peaks is 800−900 cm^{-1} for the $1B_u^+$ and $1B_u^-$ states and ~1700 cm^{-1} for the $2A_g^-$ state. Together with the above two Cars, we reanalyzed the fluorescence spectrum of lycopene[25] by introducing the additional contribution of the $1B_u^-$ fluorescence. The details of the analyses will be described below.

(a) Anhydrorhodovibrin (Figure 2a). (1) The Raman lines on the top of the $1B_u^+$ fluorescence, which are considerably broad because of a large slit width used for collecting very weak fluorescence, were subtracted by taking into account the shape of the Raman lines and the background scattering (see the shaded area in Figure 2a-1). (2) The energies of the $0 \rightarrow 0$, $0 \rightarrow 1$, and $0 \rightarrow 2$ peaks of the $1B_u^+$ fluorescence were read by inspection, and the spacings of the vibronic transition were determined to be 1200 and 1100 cm^{-1}. Then, the $1B_u^+$ ($0 \rightarrow 3$) peak was set by assuming a slightly smaller spacing (1000 cm^{-1}). (3) The energies of the apparent $0 \rightarrow 1$ and $0 \rightarrow 2$ peaks and the general profile of the $2A_g^-$ fluorescence showing a maximum around the $0 \rightarrow 2$ transition[23,25] lead us to the location of the $0 \rightarrow 0$ energy around 12 500 cm^{-1} (Figure 2a-3). (4) By the use of a pair of bumps on the shoulder of the fluorescence profile as a guide, the $0 \rightarrow 0$ and $0 \rightarrow 1$ peaks of the $1B_u^-$ fluorescence were located (Figure 2a-2). An attempt of spectral decomposition assuming the $0 \rightarrow 4$ and $0 \rightarrow 5$ peaks of the $1B_u^+$ fluorescence progression, instead, gave rise to an inflection of the fitting curve. (5) After setting the $0 \rightarrow 3$ peak of the $2A_g^-$ fluorescence and the $0 \rightarrow 2$ peak of the $1B_u^-$ fluorescence assuming the same spacings for the $0 \rightarrow 3$ and $0 \rightarrow 2$ peaks of the $1B_u^+$ fluorescence (in reference to the $0 \rightarrow 2$ and $0 \rightarrow 1$ peaks), the intensities and the bandwidths (see the above assumption iii) of all of the vibronic peaks were fit manually. Table 1a lists the energies of all of the vibronic transitions and their spacings in the $1B_u^+$, $1B_u^-$, and $2A_g^-$ fluorescence thus determined.

To give evidence for the $1B_u^-$ state, we recorded the fluorescence and electronic absorption spectra of crystalline all-*trans*-anhydrorhodovibrin dispersed in a KBr disk (concentration 2×10^{-7} M). The results are shown in Figure 3. The fluorescence spectrum excited at 420 nm (solid line) exhibits a shoulder at around 14 900 cm^{-1} on the shoulder of the strong $1B_u^+ \rightarrow 1A_g^-$ fluorescence profile. On the other hand, the

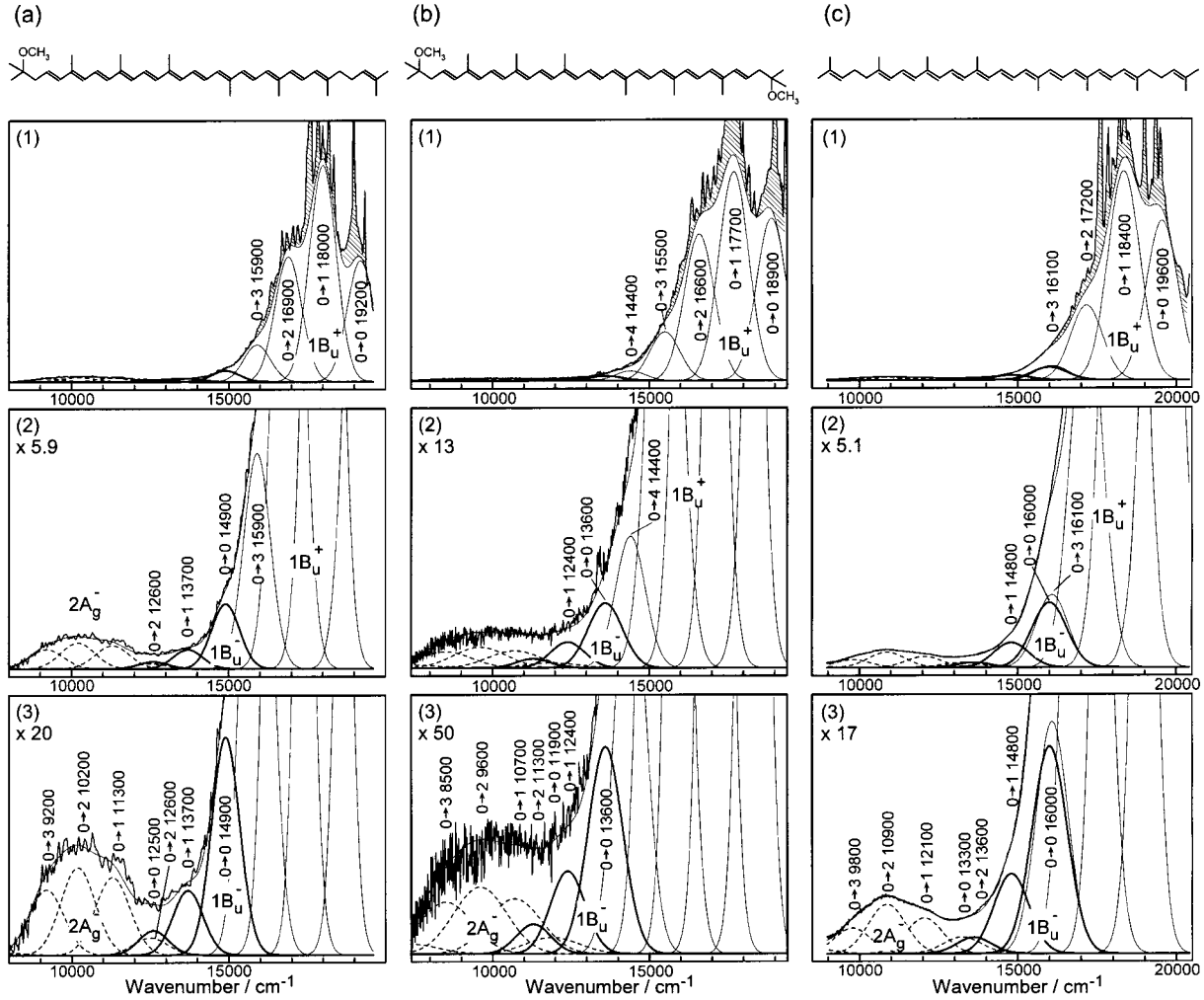

Figure 2. Fluorescence spectra of all-*trans*-Cars, i.e., (a) anhydrorhodovibrin, (b) spirilloxanthin, and (c) lycopene, recorded in *n*-hexane at 295 K (panels 1, 2, and 3 with different expansions of the same spectrum along the ordinate scale as indicated). The results of spectral decomposition into the $1B_u^+$ (weak solid line), $1B_u^-$ (strong solid line), and $2A_g^-$ (broken line) progressions are also shown. The vibronic transition and the energy of each decomposed peak are indicated.

electronic-absorption spectrum (broken line), which is free from overlap with the $1B_u^+ \leftarrow 1A_g^-$ absorption to appear above 20 000 cm^{-1}, exhibits a sharp peak at 14 900 cm^{-1}. The energy of the fluorescence shoulder and the absorption peak of the microcrystals agrees with that of the $1B_u^-$ (0)−$1A_g^-$ (0) fluorescence peak in *n*-hexane solution (see Figure 2a-3). The results support the spectral analysis described above. (The details of the experiments on the crystalline samples will be published elsewhere.)

(b) Spirilloxanthin (Figure 2b). (1) After removal of the Raman signals, the 0 → 0, 0 → 1, and 0 → 2 peaks of the $1B_u^+$ fluorescence were read by inspection to determine the spacings (1200 and 1100 cm^{-1}), and then its 0 → 3 and 0 → 4 peaks were located by assuming the latter spacing (Figure 2b-1). (2) The energy of the $2A_g^-$ (0 → 0) transition was determined to be 11 900 cm^{-1} by assuming the general profile of the $2A_g^-$ fluorescence having a maximum at the 0 → 2 transition. The same spacings as those of the $1B_u^+$ fluorescence were assumed to locate all of the vibronic peaks in the $2A_g^- \rightarrow 1A_g^-$ fluorescence progression. (3) By the use of a bump in the fluorescence profile as a guide, the $1B_u^-$ (0 → 0) peak was located, and its (0 → 1) and (0 → 2) progressions were set assuming the same spacings as in the $1B_u^+$ state (Figure 2b-2). Then, the position of the entire $1B_u^- \rightarrow 1A_g^-$ progression was adjusted manually to fit the fluorescence profile. (4) The intensities and the bandwidths of all of the three progressions were fit manually. Table 1b lists the energies of the vibronic transitions thus determined.

(c) Lycopene (Figure 2c). (1) The $1B_u^+$ and $2A_g^-$ fluorescence progressions were fixed as determined previously.[25] (2) Some modification of this previous analysis was made on the basis of an assumption that the $1B_u^+$ (0 → 3) peak is overlapped with the $1B_u^-$ (0 → 0) peak (as a first guess), the position of which was based on a linear relation of the $1B_u^-$ energy shown in Figure 1a and on the $1B_u^-$ energies of anhydrorhodovibrin and spirilloxanthin determined above. (3) A set of the $1B_u^-$ (0 → 0), (0 → 1), and (0 → 2) peaks with fixed spacings that were determined for the $1B_u^+$ fluorescence progression was assumed, and the position of the entire set was determined. Finally, the intensities and the widths of all of the vibronic peaks in this region were adjusted manually. Table 1c lists the energies of vibronic transitions thus determined.

Hereafter, we will systematically compare the energies of the $1B_u^+$, $1B_u^-$, and $2A_g^-$ states as well as the transition dipoles for the fluorescence transitions from those excited states to the $1A_g^-$ state, in the order of decreasing *n*, i.e., spirilloxanthin (*n* = 13), anhydrorhodovibrin (*n* = 12), and lycopene (*n* = 11).

The State Energies. *(a) Temperature Dependence.* A clear difference between the ionic $1B_u^+$ state and the covalent $1B_u^-$ and $2A_g^-$ states defined by Tavan and Schulten[11] has been found

TABLE 1: Energies (in cm^{-1}) of the Vibronic Transitions in the $1B_u^+$, $1B_u^-$, and $2A_g^-$ Fluorescence for All-*trans*-Cars in *n*-Hexane Solution[a]

(a) anhydrorhodovibrin		0−0	δ	0−1	δ	0−2	δ	0−3
295 K	$1B_u^+ \leftarrow 1A_g^-$	19400		20700		21900		23100
			1300		*1200*		*1200*	
	$1B_u^+ \rightarrow 1A_g^-$	19200		18000		16900		15900
			1200		*1100*		*1000*	
	$1B_u^- \rightarrow 1A_g^-$	14900		13700		12600		
			1200		*1100*			
	$2A_g^- \rightarrow 1A_g^-$	12500		11300		10200		9200
			1200		*1100*		*1000*	
150 K	$1B_u^+ \leftarrow 1A_g^-$	19100		20500		21800		23100
			1400		*1300*		*1300*	
	$1B_u^+ \rightarrow 1A_g^-$	19000		17800		16700		15700
			1200		*1100*		*1000*	
	$1B_u^- \rightarrow 1A_g^-$	14900		13700		12600		
			1200		*1100*			
	$2A_g^- \rightarrow 1A_g^-$	12500		11300		10200		9200
			1200		*1100*		*1000*	

(b) spirilloxanthin		0−0	δ	0−1	δ	0−2	δ	0−3	δ	0−4
295 K	$1B_u^+ \leftarrow 1A_g^-$	19000		20300		21600		22900		
			1300		*1300*		*1300*			
	$1B_u^+ \rightarrow 1A_g^-$	18900		17700		16600		15500		14400
			1200		*1100*		*1100*		*1100*	
	$1B_u^- \rightarrow 1A_g^-$	13600		12400		11300				
			1200		*1100*					
	$2A_g^- \rightarrow 1A_g^-$	11900		10700		9600		8500		
			1200		*1100*		*1100*			
150 K	$1B_u^+ \leftarrow 1A_g^-$	18800		20100		21400		22700		
			1300		*1300*		*1300*			
	$1B_u^+ \rightarrow 1A_g^-$	18700		17500		16400		15400		14400
			1200		*1100*		*1000*		*1000*	
	$1B_u^- \rightarrow 1A_g^-$	13600		12400		11300				
			1200		*1100*					
	$2A_g^- \rightarrow 1A_g^-$	11900		10700		9600		8600		
			1200		*1100*		*1000*			

(c) lycopene		0−0	δ	0−1	δ	0−2	δ	0−3
295 K	$1B_u^+ \leftarrow 1A_g^-$	19900		21300		22600		23900
			1400		*1300*		*1300*	
	$1B_u^+ \rightarrow 1A_g^-$	19600		18400		17200		16100
			1200		*1200*		*1100*	
	$1B_u^- \rightarrow 1A_g^-$	16000		14800		13600		
			1200		*1200*			
	$2A_g^- \rightarrow 1A_g^-$	13300		12100		10900		9800
			1200		*1200*		*1100*	
170 K	$1B_u^+ \leftarrow 1A_g^-$	19800		21200		22600		24000
			1400		*1400*		*1400*	
	$1B_u^+ \rightarrow 1A_g^-$	19500		18300		17100		16000
			1200		*1200*		*1100*	
	$1B_u^- \rightarrow 1A_g^-$	16000		14800		13600		
			1200		*1200*			
	$2A_g^- \rightarrow 1A_g^-$	13300		12100		10900		9800
			1200		*1200*		*1100*	

[a] Spacings between a pair of neighboring transitions (δ) are also shown in italic.

in the present investigation as the temperature dependence of the state energies. In spirilloxanthin (Table 1b), the $1B_u^+$ (0) energy (the energy of the $1B_u^+$ (0) → $1A_g^-$ (0) fluorescence) decreases from 18 900 to 18 700 cm^{-1} (Δ, −200 cm^{-1}) when the temperature is lowered from 295 to 150 K. On the other hand, the $1B_u^-$ (0) and the $2A_g^-$ (0) energies stay at 13 600 and 11 900 cm^{-1}, respectively. [Hereafter, the $1B_u^+$ (0), $1B_u^-$ (0), and $2A_g^-$ (0) energies will be abbreviated as the $1B_u^+$, $1B_u^-$ and $2A_g^-$ energies.] In anhydrorhodovibrin (Table 1a), the $1B_u^+$ energy is lowered from 19 200 to 19 000 cm^{-1} (Δ, −200 cm^{-1}) upon the same decrease in temperature, whereas the $1B_u^-$ and the $2A_g^-$ energies stay at 14 900 and 12 500 cm^{-1}. In lycopene (Table 1c), the $1B_u^+$ energy goes down from 19 600 to 19 500 cm^{-1} (Δ, −100 cm^{-1}) by lowering temperature from 295 to 170 K, but the $1B_u^-$ energy (16 000 cm^{-1}) and the $2A_g^-$ energy (13 300 cm^{-1}) remain unchanged.

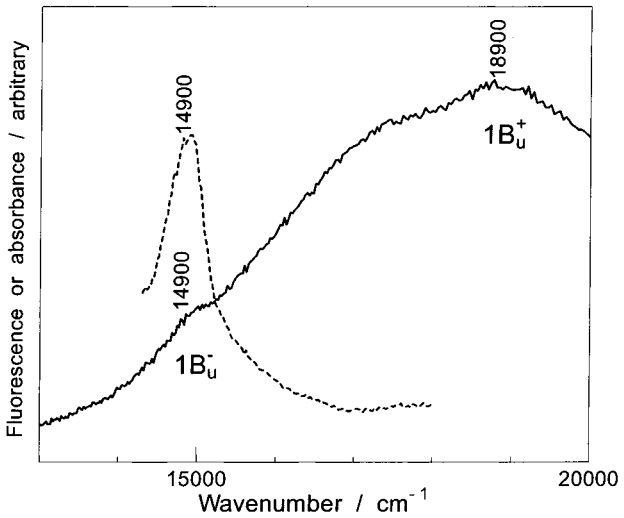

Figure 3. Fluorescence spectrum excited at 488 nm (solid line) and electronic-absorption spectrum (broken line) of crystalline all-*trans*-anhydrorhodovibrin that was dispersed in a KBr disk (concentration, 2×10^{-7} M).

The lowering of the $1B_u^+$ energy upon the lowering of the temperature can be ascribed to increase in the refractive index (n') of the solvent because of the decrease in its volume at low temperatures. It was shown that the $1B_u^+$ decreases, as a function of $(n'^2 - 1)/(n'^2 + 2)$, when the solvent polarizability increases.[29,30] The difference between the ionic $1B_u^+$ state and the covalent $2A_g^-$ state has already been found for shorter-chain Cars including all-*trans*-neurosporene, spheroidene,[23] and lycopene.[25] This trend is now generalized for the longer-chain Cars, i.e., anhydrorhodovibrin and spirilloxanthin. Most importantly, it has been shown in the present investigation that the energy of the $1B_u^-$ state exhibits no temperature dependence at all, a fact which supports the assignment of this particular excited state and justifies the above spectral analysis.

(b) Dependence on n. All of the $2A_g^-$, $1B_u^-$, and $1B_u^+$ energies of the set of Cars exhibit dependence on *n*, as a function of $1/(2n + 1)$, as shown in Figure 1b. The $2A_g^-$ energies of all-*trans*-spirilloxanthin ($n = 13$) and anhydrorhodovibrin ($n = 12$), i.e., 11 900 and 12 500 cm^{-1}, sit on the extrapolated part of the regression line proposed in a previous investigation, i.e., $E(2A_g^-) = 220\,550/(2n + 1) + 3700$ cm^{-1};[25] by insertion of $n = 12$ and 13, this equation predicts the $2A_g^-$ energies of those Cars to be 11 869 and 12 522 cm^{-1}, in agreement with the proposed values.

The $1B_u^-$ energies of the present Cars, i.e., all-*trans*-spirilloxanthin, anhydrorhodovibrin, and lycopene, give rise to an regression line, i.e., $E(1B_u^-) = 370\,981/(2n + 1) - 70$ cm^{-1}, although additional data for shorter-chain Cars are necessary to establish this linear relation. It is interesting to point out that the ordering of the state energies, i.e., $2A_g^-$ (S_1) < $1B_u^-$ (S_2) < $3A_g^-$ (S_3), seems to hold true for all of the photosynthetic Cars having $n = 9-13$.[8]

The $1B_u^+$ energies determined by both the $1B_u^+ \leftarrow 1A_g^-$ absorption and the $1B_u^+ \rightarrow 1A_g^-$ fluorescence give rise to parallel regression lines. However, the Stokes shift seems to decrease when *n* increases; it is 300 cm^{-1} in all-*trans*-neurosporene ($n = 9$), spheroidene ($n = 10$),[23] and lycopene ($n = 11$), 200 cm^{-1} in anhydrorhodovibrin ($n = 12$), and 100 cm^{-1} in spirilloxanthin (present results).

The mutual arrangement of all of the regression lines (positions and slopes) for Cars in solution that have been

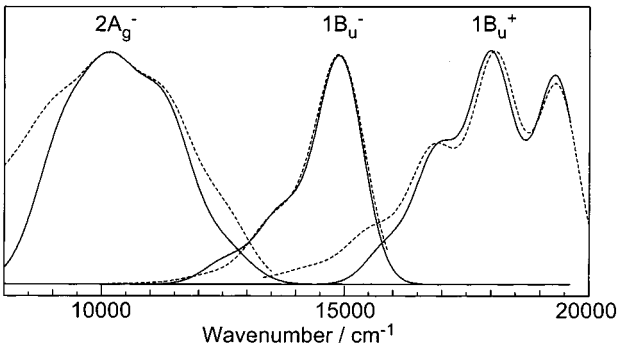

Figure 4. Simulation of the normalized $1B_u^+$, $1B_u^-$, and $2A_g^-$ fluorescence progressions by shifting the harmonic potentials along the Q_1 (C=C stretching) and Q_2 (C−C stretching) coordinates. A sum of the vibronic peaks obtained by spectral decomposition (solid line) and the result of simulation (broken line) for each fluorescence is indicated.

determined in the present investigation by electronic-absorption and fluorescence spectroscopy (Figure 1b) roughly parallels that for crystalline Cars that were determined by measurements of resonance-Raman excitation profiles (Figure 1a). The difference noticed is that the positions are higher and the slopes are gentler in Cars in solution.

The $1B_u^-$ energies of the present long-chain Cars suggest that the singlet-energy transfer from this state to the Q_y state of BChl is energetically feasible. On the other hand, their $2A_g^-$ energies suggest that the singlet-energy transfer from this state to the Q_y state of BChl may not be efficient.

Simulation of the Fluorescence Spectra and Determination of the Shifts of Excited-State Potentials. In all-*trans*-anhydrorhodovibrin, we have succeeded in proving the $1B_u^-$ (0) position by the use of both fluorescence (in *n*-hexane) and electronic-absorption (in crystals) spectroscopy. To determine the shifts of the $1B_u^+$, $1B_u^-$, and $2A_g^-$ potential minima (in reference to the $1A_g^-$ potential minimum) along the ν_1 (C=C stretching) and ν_2 (C−C stretching) normal coordinates, Q_1 and Q_2, we have attempted to simulate each of the $1B_u^+$, $1B_u^-$, and $2A_g^-$ fluorescence progressions obtained as a sum of the vibronic components determined by the above spectral decomposition. We used a method described previously,[24] and the results are shown in Figure 4. Each solid line shows the sum of the relevant vibronic components, and each broken line shows the result of simulation by the use of the ν_1 and ν_2 Raman frequencies in the $1A_g^-$ state, i.e., 1512 and 1153 cm^{-1}, as well as the shifts of the potential minima along the Q_1 and Q_2 normal coordinates, i.e., Δ_1 and Δ_2, the latter of which were used as fitting parameters. The maxima of the $1B_u^+$, $1B_u^-$, and $2A_g^-$ fluorescence are normalized, and the effect of self-absorption is corrected for the $1B_u^+$ (0) → $1A_g^-$ (0) fluorescence peak. The rapid decline of the $2A_g^-$ fluorescence on the low-energy side is probably due to the loss of the sensitivity of the detector. The (Δ_1, Δ_2) values determined by this simulation were (0.9, 1.3), (0.5, 0.6), and (1.2, 1.9) for the $1B_u^+$, $1B_u^-$, and $2A_g^-$ states, respectively. The profiles of the three fluorescence profiles are roughly reproduced by the simulation using only two normal modes.

Figure 5 depicts a pair of potential diagrams for the $1B_u^+$, $1B_u^-$, and $2A_g^-$ states (in reference to the $1A_g^-$ state) along the (1) Q_1 and (2) Q_2 normal coordinates. The potentials are drawn based on the following observations and assumptions: (i) The $1B_u^+$ (0), $1B_u^-$ (0), and $2A_g^-$ (0) energies are as determined in the previous section. It is assumed that the fluorescence transition from each electronic state takes place after complete relaxation to the bottom of the potential (the v = 0 level). (ii) The same harmonic potentials are assumed for all of the electronic states. The shifts of the potential minima for the $1B_u^+$, $1B_u^-$, and $2A_g^-$ states are as determined by the above simulation. It is assumed that the potential minimum shifts upon excitation to the positive direction along the Q_1 and Q_2 coordinates.

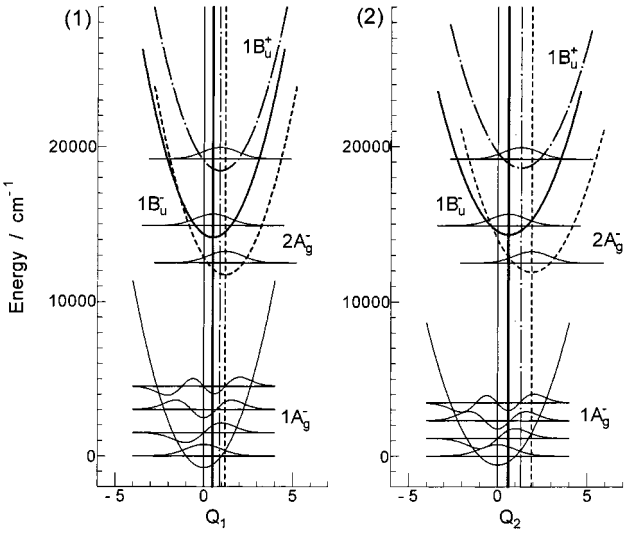

Figure 5. Pair of potential diagrams for the $1B_u^+$, $1B_u^-$, and $2A_g^-$ states of all-*trans*-anhydrorhodovibrin along the (1) Q_1 and (2) Q_2 normal coordinates. See text for the details.

Such potential diagrams, when obtained for all of the different Cars, will be useful to determine the detailed mechanisms of internal conversion.

Transition Dipoles. The oscillator strength of an absorptive transition can be obtained by

$$f = 4.32 \times 10^{-9} n_r \int \epsilon(\tilde{\nu})\, d\tilde{\nu} \qquad (1)$$

where n_r is the refractive index of the solvent and $\epsilon(\tilde{\nu})$ is the molar extinction coefficient as a function of wavenumber $\tilde{\nu}$. On the other hand, the oscillator strength can be related to the transition dipole moment (hereafter abbreviated as "the transition dipole") by

$$f = \frac{8\pi^2 m_e c \tilde{\nu}_{nm}}{3he^2} |\mu_{nm}|^2 \qquad (2)$$

where m_e and e are the mass and the electronic charge of electron, h is Plank's constant, c is the speed of light, $\tilde{\nu}_{nm}$ is the energy of the particular ($n \leftarrow m$) transition in cm^{-1}, and μ_{nm} is the corresponding transition dipole. Then, the transition dipole (μ_{nm} in Debye) can be given as

$$|\mu_{nm}| = 1458.4 \sqrt{\frac{f}{\tilde{\nu}_{nm}}} \qquad (3)$$

The rate of emission (k_{em}) is also related to the transition dipole as

$$k_{em} = \frac{64\pi^4 n_r |\mu_{nm}|^2}{3he^2} \tilde{\nu}_{nm}^{\ 3} \qquad (4)$$

On the other hand, the emission ratio can be expressed by using the quantum yield of fluorescence ϕ and the excited-state lifetime τ as

TABLE 2: Relative Quantum Yields of Fluorescence (ϕ), the Lifetimes (τ), the State Energies (ν), the Molar Extinction Coefficients (ϵ), the Transition Dipole Moments (μ), and the Oscillator Strengths (f/n) for the $1B_u^+$ (S_3), $1B_u^-$ (S_2), and $2A_g^-$ (S_1) States of All-*trans*-spirilloxanthin, Anhydrorhodovibrin, and Lycopene in *n*-hexane Solution

	(%)[a]		(ps)[b]			(cm^{-1})			(M^{-1} cm^{-1})[c]	(D)					
	ϕ_{S_2}/ϕ_{S_3}	ϕ_{S_1}/ϕ_{S_3}	τ_{S_3}	τ_{S_2}	τ_{S_1}	ν_{S_3}	ν_{S_2}	ν_{S_1}	ϵ_{S_3} at the maximum	μ_{S_3}	μ_{S_2}	μ_{S_1}	f_{S_3}/n	f_{S_2}/n	f_{S_1}/n
spirilloxanthin	1.4	1.2	0.18	0.14	1.3	18 900	13 600	11 900	151 000	16.8 (1)	3.72 (0.22)	1.37 (0.082)	2.50 (1)	0.09 (0.036)	0.010 (0.004)
anhydrorhodovibrin	3.2	3.1	0.10	0.09	2.2	19 200	14 900	12 500	171 000	17.4 (1)	4.76 (0.27)	1.24 (0.071)	2.73 (1)	0.16 (0.059)	0.009 (0.003)
lycopene	4.2	1.9	0.17	0.16	4.7	19 600	16 000	13 300	181 500	17.2 (1)	4.94 (0.29)	0.80 (0.047)	2.74 (1)	0.18 (0.066)	0.004 (0.002)

[a] Effect of self-absorption in the $1B_u^+ \rightarrow 1A_g^-$ fluorescence is corrected. [b] T. Inaba, J.-P. Zhang, R. Fujii, T. Ishikawa, and Y. Koyama, unpublished results. [c] P. Qian, T. Mizoguchi, Y. Sadakage, R. Fujii, T. Ishikawa, and Y. Koyama, unpublished results.

$$k_{em} = \frac{\phi}{\tau} \tag{5}$$

Combining the above two equations, we obtain

$$\frac{\mu_1}{\mu_2} = \left(\frac{\phi_1 \tau_2 \tilde{\nu}_2^{\,3}}{\phi_2 \tau_1 \tilde{\nu}_1^{\,3}}\right)^{1/2} \tag{6}$$

where 1 and 2 refer to the pair of electronic states.

Because we have recently determined, for spirilloxanthin, anhydrorhodovibrin, and lutein, (i) the molar extinction coefficients and the spectra of the $1B_u^+ \leftarrow 1A_g^-$ absorption (P. Qian, T. Mizoguchi, Y. Sadakage, R. Fujii, T. Ishikawa and Y. Koyama, unpublished results), (ii) the lifetimes of the $1B_u^+$, $1B_u^-$, and $2A_g^-$ states (T. Inaba, J.-P. Zhang, R. Fujii, T. Ishikawa and Y. Koyama, unpublished results), and (iii) the relative quantum yields and the energies for fluorescence from those states to the $1A_g^-$ state (the present investigation), we can now calculate, by the use of eqs 1, 3, and 6, the transition dipoles for the $1B_u^+ \rightarrow 1A_g^-$, $1B_u^- \rightarrow 1A_g^-$, and $2A_g^- \rightarrow 1A_g^-$ transitions (hereafter, abbreviated as the $1B_u^+$, $1B_u^-$, and $2A_g^-$ transition dipoles, respectively).

Table 2 shows the results: The values of the $1B_u^+$ (S_3) transition dipoles are similar to one another irrespective of the number of conjugated double bonds, *n*. The $1B_u^-$ (S_2) transition dipole decreases, whereas the $2A_g^-$ (S_1) transition dipole increases systematically when *n* increases from lycopene to spirilloxanthin. Most importantly, the transition dipoles from the $1B_u^-$ state, relative to that from the strongly optically allowed $1B_u^+$ state, range as high as 20−30%. It has been shown that the singlet-energy transfer from the $2A_g^-$ state of Car to the Q_y state of BChl takes place through Coulombic mechanism for lycopene in the LH2 complex from *Rhodospirillum molischianum*[15] even though the relative transition dipole estimated here is only 5%. Therefore, there remains a chance of singlet energy transfer from the $1B_u^-$ state for the present longer-chain Cars (see Figure 1b), although the $1B_u^-$ lifetime is more than 1 order of magnitude shorter than that of the $2A_g^-$ state (see the fourth and fifth columns in Table 2).

The oscillator strength of the $1B_u^+$ state decreases gradually when *n* increases. On the other hand, the oscillator strength of the $1B_u^-$ state decreases, whereas that of the $2A_g^-$ state increases. The ratio of the $1B_u^+$, $1B_u^-$, and $2A_g^-$ oscillator strengths, $1:10^{-2}:10^{-3}$, determined in the present investigation (Table 2) agrees with that predicted in the measurements of resonance-Raman excitation profiles.[8] However, a close comparison of the absolute values needs to consider the symmetry of the Car molecules as well (see Figure 2 for their structures).

Conclusions

Fluorescence spectra of all-*trans*-anhydrorhodovibrin ($n = 12$) and spirilloxanthin ($n = 13$) were recorded and analyzed together with that of all-*trans*-lycopene ($n = 11$) reported previously.[25] The $2A_g^-$ energies of the former two Cars (12 500 and 11 900 cm^{-1}) confirmed the dependence of the $2A_g^-$ energy on $1/(2n + 1)$ which had been proposed previously on the basis of the $2A_g^-$ energies of shorter-chain Cars ($n = 7-11$), i.e., $E(2A_g^-) = 220\,550/(2n + 1) + 3700$ cm^{-1}.[25]

In all-*trans*-anhydrorhodovibrin, the $1B_u^-$ state was evidenced by both fluorescence and electronic-absorption spectroscopy. Therefore, the shifts of the $1B_u^+$, $1B_u^-$, and $2A_g^-$ potentials along the C=C and C−C stretching normal coordinates (Δ_1, Δ_2) were determined to be (0.9, 1.3), (0.5, 0.6), and (1.2, 1.9), respectively, on the basis of the simulation of the $1B_u^+$, $1B_u^-$, and $2A_g^-$ fluorescence progressions.

The $1B_u^-$ (0) energies of all-*trans*-spirilloxanthin, anhydrorhodovibrin, and lycopene gave rise to a regression line, $E(1B_u^-) = 370\,981/(2n + 1) - 70$ cm^{-1}, a relation which is to be refined in the future.

A set of transition dipoles were determined by the use of the $1B_u^+ \leftarrow 1A_g^-$ absorption and the $1B_u^+ \rightarrow 1A_g^-$, $1B_u^- \rightarrow 1A_g^-$, and $2A_g^- \rightarrow 1A_g^-$ fluorescence of all-*trans*-spirilloxanthin, anhydrorhodovibrin, and lycopene. The $1B_u^-$ and $2A_g^-$ transition dipole moments were in the ranges of 20−30% and 5−8% of the $1B_u^+$ transition dipole moment (∼17 D) for the above three Cars.

Acknowledgment. The authors would like to thank Dr. Jian-Ping Zhang, in this laboratory, for reading the manuscript and stimulating discussion. The strain of *Allochromatium vinosum* was a gift from Prof. Keizo Shimada of Tokyo Metropolitan University. Financial supports from the Science Research Promotion Fund and from the Japan Society for the Promotion of Science are gratefully acknowledged. R.F. has been supported by a JSPS fellowship for Japanese junior scientists and a grant-in-aid from the Ministry of Education, Science, Sports and Culture, Japan (No. 7725).

References and Notes

(1) Frank, H. A.; Cogdell, R. J. *Carotenoids in Photosynthesis*, 1st ed.; Chapman & Hall: London, 1993; Chapter 8.
(2) Koyama, Y.; Kuki, M.; Andersson, P. O.; Gillbro, T. *Photochem. Photobiol.* **1996**, *63*, 243.
(3) Pariser, R. *J. Chem. Phys.* **1956**, *24*, 250.
(4) Callis, P. R.; Scott, T. W.; Albrecht, A. C. *J. Chem. Phys.* **1983**, *78*, 16.
(5) Sashima, T.; Nagae, H.; Kuki, M.; Koyama, Y. *Chem. Phys. Lett.* **1999**, *299*, 187.
(6) Kuki, M.; Nagae, H.; Cogdell, R. J.; Shimada, K.; Koyama, Y. *Photochem. Photobiol.* **1994**, *59*, 116.
(7) Zhang, J.-P.; Inaba, T.; Koyama, Y. *J. Mol. Struct.* Submitted for publication
(8) Sashima, T.; Koyama, Y.; Yamada, T.; Hashimoto, H. *J. Phys. Chem. B* **2000**, *104*, 5011.
(9) Ritz, T.; Damjanovic, A.; Schulten, K.; Zhang, J.-P.; Koyama, Y. *Photosynth. Res.* In press.
(10) Tavan, P.; Shulten, K. *J. Chem. Phys.* **1986**, *85*, 6602.

(11) Tavan, P.; Schulten, K. *Phys. Rev.* **1987**, *36*, 4337.
(12) Zhang, J.-P.; Inaba, T.; Watanabe, Y.; Koyama, Y. *Chem. Phys. Lett.* **2000**, *331*, 54.
(13) Zhang, J.-P.; Inaba, T.; Watanabe, Y.; Koyama, Y. *Chem. Phys. Lett.* **2000**, *332*, 351.
(14) Förster, T. *Discuss. Faraday Soc.* **1959**, *27*, 7.
(15) Zhang, J.-P.; Fujii, R.; Qian, P.; Inaba, T.; Mizoguchi, T.; Koyama, Y.; Onaka, K.; Nagae, H. *J. Phys. Chem. B* **2000**, *104*, 3683.
(16) Chynwat, V.; Frank, H. A. *Chem. Phys.* **1995**, *194*, 237.
(17) Frank, H. A.; Desamero, R. Z. B.; Chynwat, V.; Gebhard, R.; Hoef, I.; Jansen, F. J.; Lugtenburg, J.; Gosztola, D.; Wasielewski, M. R. *J. Phys. Chem.* A **1997**, *101*, 149.
(18) Andersson, P. O.; Bachilo, S. M.; Chen, R.-L.; Gillbro, T. *J. Phys. Chem.* **1995**, *99*, 16199.
(19) Frank, H. A.; Bautista, J. A.; Josue, J. S.; Young, A. J. *Biochemistry* **2000**, *39*, 2831.
(20) Polívka, T.; Herek, J. L.; Zigmantas, D.; Åkerlund, H.-E.; Sundström, V. *Proc. Natl. Acad. Sci. U.S.A.* **1999**, *96*, 4914.
(21) Krueger, B. P.; Yom, J.; Walla, P. J.; Fleming, G. R. *Chem. Phys. Lett.* **1999**, *310*, 57.
(22) DeCoster, B.; Christensen, R. L.; Gebhard, R.; Lugtenburg, J.; Farhoosh, R.; Frank, H. A. *Biochim. Biophys. Acta* **1992**, *1102*, 107.
(23) Fujii, R.; Onaka, K.; Kuki, M.; Koyama, Y.; Watanabe, Y. *Chem. Phys. Lett.* **1998**, *288*, 847.
(24) Onaka, K.; Fujii, R.; Nagae, H.; Kuki, M.; Koyama, Y.; Watanabe, Y. *Chem. Phys. Lett.* **1999**, *315*, 75.
(25) Fujii, R.; Onaka, K.; Nagae, H.; Koyama, Y.; Watanabe, Y. *J. Luminesc.* **2001**, *92*, 213.
(26) Sashima, T.; Shiba, M.; Hashimoto, H.; Nagae, H.; Koyama, Y. *Chem. Phys. Lett.* **1998**, *290*, 36.
(27) Bose, S. K. *Bacterial Photosynthesis*; The Antioch Press: Yellow Springs, OH, 1963; p 507.
(28) Miki, Y.; Kameyama, T.; Koyama, Y.; Watanabe, Y. *J. Phys. Chem.* **1993**, *97*, 6142.
(29) Andersson, P. O.; Gillbro, T.; Ferguson, L.; Cogdell, R. J. *Photochem. Photobiol.* **1991**, *54*, 353.
(30) Nagae, H.; Kuki, M.; Cogdell, R. J.; Koyama, Y. *J. Chem. Phys.* **1994**, *101*, 6750.